International Journal of Heat and Mass Transfer 183 (2022) 122240

Contents lists available at ScienceDirect

International Journal of Heat and Mass Transfer

journal homepage: www.elsevier.com/locate/hmt

Constructal design of a circular micro-channel Stirling regenerator based on exergy destruction minimization

Minjie Yu, Chunyu Shi, Junhao Xie, Peng Liu, Zhichun Liu, Wei Liu*

School of Energy and Power Engineering, Huazhong University of Science and Technology, Wuhan 430074, China

ARTICLE INFO

Article history:
Received 28 July 2021
Revised 15 October 2021
Accepted 8 November 2021
Available online 21 November 2021

Keywords:
Stirling engine
Micro-channel regenerator
Constructal design
Exergy destruction minimization

ABSTRACT

Regenerator is a key component in Stirling engines, and its characteristics have a significant influence on engine performance. Herein, subjected to the global constraints of the fixed total volume and porosity, constructal design of a circular micro-channel regenerator was conducted to achieve its optimal structures. The total exergy destruction rate in the irreversible regenerative process, which includes three types of individual exergy destruction contributions caused by the heat transfer with a finite temperature difference, flow resistance, and axial heat conduction of the solid matrix, was adopted as the optimization objective. The optimal channel diameter was obtained, and the effects of the regenerator inner radius, total volume of regenerators, regenerator porosity, engine speed, piston phase angle, hot part temperature, charge pressure, and thermal conductivity ratio due to the segmentation of regenerators on the optimization results were analyzed. The results show that the total exergy destruction rate offers a minimum at a relatively low channel diameter of around 0.5 mm under the given parameter values. All the parameters studied have an obvious effect on the minimum total exergy destruction rate, and the regenerator inner radius, total volume and porosity of regenerators, and engine speed also have an evident influence on the optimal structure of the regenerator. These indicate that the regenerator performance can be further improved by selecting appropriate global geometric parameter values of regenerators and operating parameter values of engines. The findings of this study can provide some guidelines for the optimal design of micro-channel regenerators and the performance improvement of Stirling engines.

© 2021 Elsevier Ltd. All rights reserved.

1. Introduction

Clean renewable energy sources such as solar, wind, geothermal, and biomass energy are regarded as good substitutes to fossil fuels for alleviating environment-related problems [1]. As an external combustion engine, the Stirling engine can operate in various external heat sources and thus has the potential for renewable energy utilization [2]. However, the high irreversible losses inside the Stirling engine significantly limit its output performance and hinder it from being extensively applied [3]. Therefore, it is essential to optimize the design of Stirling engines and improve the engine performance so as to promote their application.

The regenerator is one of the core components in Stirling engines, which plays a crucial role in ensuring the efficient operation of the engine [4]. As a heat storage device, the regenerator periodically absorbs and releases heat with the oscillating gas. Consequently, the heat input through the heater is considerably reduced, and thus the thermal efficiency of the engine is improved. A study by Tavakolpour et al. [5] showed that the thermal efficiency obtained by the engine with an ideal regenerator was 6 times higher than that of the engine without a regenerator. Hence, the design of an efficient regenerator is of vital importance to the performance improvement of Stirling engines. Currently, in most Stirling engines, the matrix types of regenerators are the traditional porous media such as metal foam, random fiber, and woven screen. A great many works have been carried out to investigate the pressure drop [6–11] and thermal [12–18] characteristics of these regenerators in the steady or oscillating flow, as well as to explore the effects of their parameter variations on engine performance [19–24]. These studies indicate that an excellent thermal performance is obtained for the porous regenerators owing to their high convective heat transfer and large specific surface area. Nevertheless, the cross-flow of the gas guided by the porous matrix generates numerous flow separation and vortex structures, thus resulting in a high flow loss that will degrade the power output of Stirling engines. Consequently, a new type of regenerator with low flow resistance is required for avoiding the deterioration of engine performance.

From the perspective of the arrangement of the matrix surface relative to the gas flow direction, the regenerator with the matrix

* Corresponding author.
E-mail address: w_liu@hust.edu.cn (W. Liu).

https://doi.org/10.1016/j.ijheatmasstransfer.2021.122240
0017-9310/© 2021 Elsevier Ltd. All rights reserved.

Nomenclature

a	inner and outer clearance of the regenerator, m
A	area, m^2
$A()$, $B()$, $X()$, $Y()$	non-linear combinations of zeroth-order Kelvin functions
A_0	cross-section area of a single channel, m^2
A_f	total flow cross-section area, m^2
B	piston stroke, m
bei, ber	zeroth-order Kelvin functions
C_1, C_2	intermediate variables
C_f	friction factor
C_p	specific heat, J/(kg•K)
CVC	clearance volume in the compression chamber, m^3
CVE	clearance volume in the expansion chamber, m^3
d_0	micro-channel diameter, m
d_b	cylinder bore, m
E_{xd}	transient total exergy destruction, W
$E_{xd,c}$	transient exergy destruction due to the axial heat conduction of the solid matrix, W
$E_{xd,f}$	transient exergy destruction due to the flow resistance, W
$E_{xd,h}$	transient exergy destruction due to the heat transfer with a finite temperature difference, W
f	engine frequency, Hz
F	total drag force of the gas, N
F_R	relative gas displacement ratio
h_α	average heat transfer coefficient, W/(m^2•K)
$h_{\alpha,x}$	local heat transfer coefficient, W/(m^2•K)
J_1, J_2	intermediate variables
k	thermal conductivity, W/(m•K)
KS	thermal conductivity ratio due to the segmentation of regenerators
L	regenerator length, m
N	total number of micro-channels
n	engine speed, rpm
n_r	micro-channel number per row
Nu	Nusselt number
p_0	charge pressure, Pa
Pr	Prandtl number
Q_α	heat flux in the gas-solid interface, W
r	radial position, m
r_0	micro-channel radius, m
R_0	axial thermal resistance of the solid matrix, K/W
r_1	inner radius of the regenerator, m
r_2	outer radius of the regenerator, m
R_C	total axial contact thermal resistance produced by the segmentation of the solid matrix, K/W
Re	hydraulic Reynolds number
Re_w	kinetic Reynolds number
R_g	gas constant, J/(kg•K)
S_c	transient entropy generation due to the axial heat conduction of the solid matrix, W/K
S_h	transient entropy generation due to the heat transfer with a finite temperature difference, W/K
T	temperature, K
T_0	ambient temperature, K
t_{blow}	blow time, s
u	gas velocity, m/s
V	total volume of the regenerator, m^3
V_f	channel volume of the regenerator, m^3
V_{SC}	compression swept volume, m^3
V_{SE}	expansion swept volume, m^3
x	axial position, m

Greek symbols

α	crank angle, °
α_0	initial crank angle, °
β	intermediate variable
γ	modified Womersley number
δ_{a1}	minimum circumferential interval, m
δ_{a2}	maximum circumferential interval, m
δ_r	radial interval, m
δ_T	thermal penetration depth, m
θ	central angle between two adjacent rows of micro-channels, °
Λ	phase angle between the average gas velocity in the regenerator and the piston speed of the compression chamber, °
λ	Womersley number
μ	viscosity, Pa•s
ρ	density, kg/m^3
φ	regenerator porosity
ψ	piston phase angle, °
ω	angular velocity, rad/s

Subscripts

ave	volume-average
c	compression chamber or cold part of Stirling engines
cyc	cycle
e	expansion chamber
h	hot part of Stirling engines
m	cross-sectional average
max	maximum
mi	minimum
mmi	double minimum
o	optimal
oo	double optimal
s	solid matrix

Superscripts

'	derivative
^	dimensionless
·	rate
eff	effective

surface parallel to the flow direction has the lowest flow resistance theoretically [25]. With the advance of precision machining techniques, this type of parallel geometry regenerator has attracted the interest of plenty of researchers. Some effort has been expended in developing and investigating new parallel geometry regenerators with different structures such as the segmented-involute-foil regenerators [26,27], parallel wire regenerators [28], layered-plate regenerators [29], pin-array stacked regenerators [30], robust foil regenerators [31], and regularly shaped micro-channel regenerators [25,32–34]. Therein, the circular micro-channel regenerator proposed by Alfarawi et al. [33] was shown to produce a low pressure drop and offer great potential for generating high power output. However, up to now, only the flow resistance and heat transfer performance of the circular micro-channel regenerators with different channel diameters were studied based on the steady and

single-blow methods. Other important geometric and operating parameters and the mutual constraints between different parameters have not been taken into account. Additionally, there has been no work concerning a comprehensive and rigorous optimization of the circular micro-channel regenerators, which is momentous to guide the design of regenerators with high performance. Therefore, this study is devoted to the optimization of various parameters for the circular micro-channel regenerator.

Generally, regenerator optimization is based on classical thermodynamics [21] and parameter exhaustive analyses [35]. These optimization methods mainly focus on the performance improvement of the regenerators, while the global sizes of the regenerators are not constrained. However, the total volume of the regenerator in the actual Stirling engine is limited by the overall structure layout and cost of the engine. In addition, to ensure the rationality of the optimization, the porosity of the regenerators with different geometric dimensions needs to be constant as well. With these constraints, the structure optimization of the regenerators cannot be achieved by classical optimization methods. Consequently, constructal theory considering the global constraints is introduced in this paper to optimize the regenerators. In 1996, Bejan [36] first proposed constructal theory by studying the organization of street networks. The essence of constructal theory is covered by a principle called constructal law, which is stated as: "For a finite-size flow system to persist in time (to live) it must evolve such that it provides greater and greater access to the currents that flow through it" [37]. As described in the constructal law, different from the classical optimization methods, constructal theory focuses on the geometry evolutions of finite-size systems. Over the last few decades, it has been widely applied in designing and optimizing various engineering equipment with global constraints, such as fins [38,39], cavities [40], channel networks [41,42], heated bodies [43], heat exchangers [44,45], power generators [46,47], and turbines [48]. Whereas, no attempt to optimize the regenerator structure on the basis of constructal theory has been reported so far. Hence, one of the innovations of this paper is the first time to conduct the structure optimization of the regenerators using constructal theory.

To reflect the overall performance of regenerators, a few effective evaluation criteria were put forward, which can be roughly divided into two categories according to the research perspective. At the level of components, the regenerator is treated as an individual heat exchanger, and the criteria such as the heat transfer coefficient and friction factor are usually employed to quantify the regenerator performance. While from the perspective of engines, the irreversibility is adopted to characterize the effect of the regenerator (or regenerative process) on the performance of Stirling engines. In this sense, when other engine parameters are kept constant, the decrease in the irreversibility of the regenerator means the improvement of the engine performance. At present, the physical quantities commonly used to represent the irreversibility of processes include entropy generation [49] and exergy destruction [50], etc. Among them, the exergy destruction is a measure of the available energy loss of systems due to the irreversibility of processes [51], which has the same dimension as energy, and thus its physical implication is readily accessible. To guide the technique development, a principle of exergy destruction minimization was proposed by Liu et al. [52]. In the past several years, some works have been done to analyze and optimize the performance of devices [53,54] and systems [55] by minimizing the exergy destruction. However, to the best of our knowledge, few studies have been published for the structure optimization of regenerators based on exergy destruction minimization to date.

Based on the above considerations, this study aims to optimize the structures of the circular micro-channel regenerators based on constructal theory. The minimization of the total exergy destruction of the regenerators, covering the irreversible losses caused by the heat transfer with a finite temperature difference, flow resistance, and axial heat conduction of the solid matrix, was taken as the optimization objective. With the fixed total volume and porosity of the regenerators, the relationship between the total exergy destruction rate and the geometric and operating parameters was established. Beside, some local constraints between the different parameters of the regenerators were also considered. In the whole constructal optimization, the channel diameter of regenerators was selected as the main optimization variable. The effects of other important parameters such as the regenerator inner radius, total volume of regenerators, regenerator porosity, engine speed, piston phase angle, hot part temperature, charge pressure, and thermal conductivity ratio due to the segmentation of regenerators on the optimization results were investigated and analyzed.

2. Mathematical model of regenerator

2.1. Regenerator geometry description

Fig. 1 presents the global 3-D model of the circular micro-channel regenerator, and Fig. 2 gives the schematic diagram of the local cross-section of the regenerator. The regenerator shows an annular overall configuration with the length, inner and outer radii of L, r_1, and r_2, respectively. Numerous rows of circular micro-channels parallel to the axial direction are distributed along the radial direction of the regenerator, and the central angle between two adjacent rows is θ. Each row comprises n_r micro-channels with a diameter of d_0. The inner and outer clearance of the regenerator is denoted by a, which has a constant value of 1 mm.

According to the geometric relationship, the radial, minimum and maximum circumferential intervals between adjacent channels δ_r, δ_{a1}, and δ_{a2} can be respectively expressed as:

$$\delta_r = \frac{r_2 - r_1 - 2a - n_r d_0}{n_r - 1} \tag{1}$$

$$\delta_{a1} = \frac{\theta}{360} 2\pi r_1 - d_0 \tag{2}$$

$$\delta_{a2} = \frac{\theta}{360} 2\pi r_2 - d_0 \tag{3}$$

The total heat transfer area of the regenerator is calculated as:

$$A = \pi d_0 L N = \frac{360\pi d_0 n_r L}{\theta} \tag{4}$$

where N denotes the number of micro-channels.

The total volume and channel volume of the regenerator are respectively determined as:

$$V = \pi \left(r_2^2 - r_1^2\right) L \tag{5}$$

$$V_f = \frac{\pi d_0^2}{4} L N = \frac{90\pi d_0^2 n_r L}{\theta} \tag{6}$$

Accordingly, the porosity of the micro-channel regenerator can be defined as:

$$\varphi = \frac{V_f}{V} = \frac{90 d_0^2 n_r}{\theta\left(r_2^2 - r_1^2\right)} \tag{7}$$

As previously mentioned, to ensure a finite global geometric dimension and a reasonable structure optimization for the regenerator, the constructal design of the present study is conducted under the fixed total volume and porosity of the regenerator, as described below.

$$V = \text{Constant} \tag{8}$$

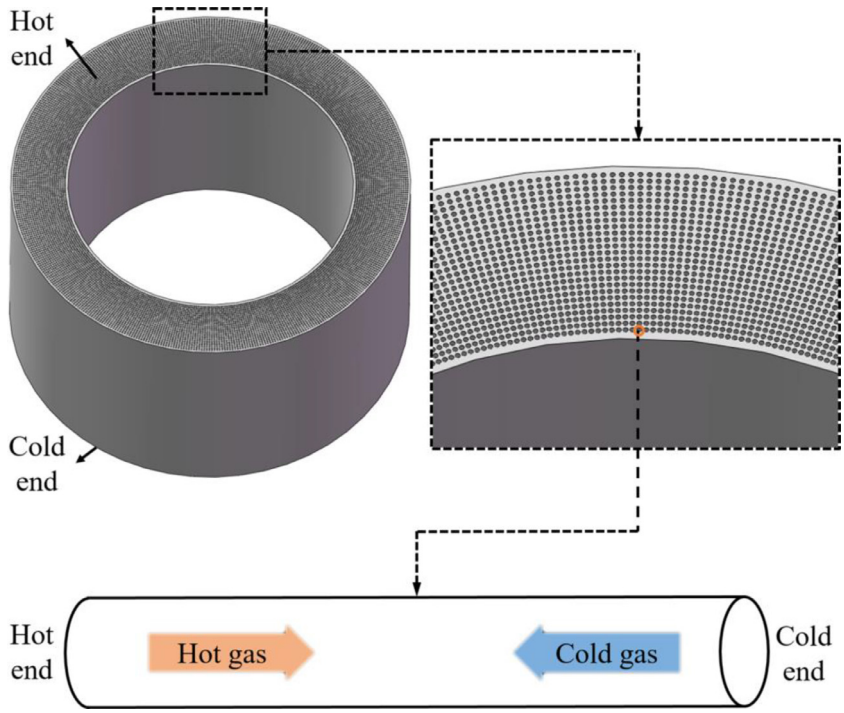

Fig. 1. Schematic of the global 3-D model for the circular micro-channel regenerator.

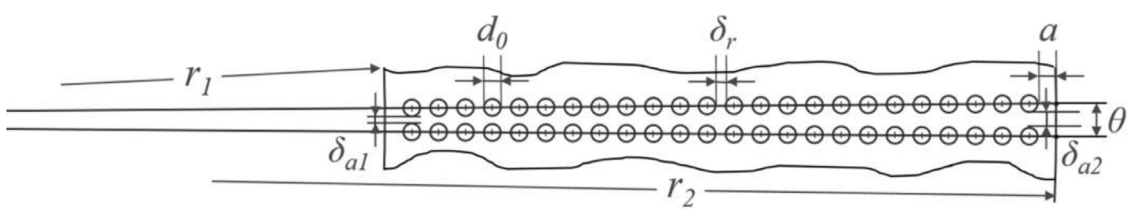

Fig. 2. Schematic of the local cross-section for the circular micro-channel regenerator.

$$\varphi = \text{Constant} \tag{9}$$

Beside, some local constraints are taken into account to successfully obtain a regenerator with the potential of achieving high performance. One local constraint is that a minimum circumferential interval greater than 0 is required for avoiding interference between micro-channels.

$$\delta_{a1} > 0 \tag{10}$$

The other one is that the radial and maximum circumferential intervals should be equal to the thermal penetration depth δ_T, which is the distance that heat can diffuse through the solid matrix during a blow time $t_{blow} = 1/(\pi f)$, where f is the engine frequency.

$$\delta_r, \delta_{a2} = \delta_T \tag{11}$$

where the thermal penetration depth δ_T is defined as [33]:

$$\delta_T = \sqrt{\frac{k_s}{\pi f \rho_s C_{ps}}} \tag{12}$$

where k_s, ρ_s, and C_{ps} are the thermal conductivity, density, and specific heat of the solid matrix, respectively.

Based on the above geometric constraints, when two of the six critical dimension parameters, namely, regenerator length L, regenerator inner radius r_1, regenerator outer radius r_2, channel diameter d_0, channel central angle θ, and channel number per row n_r, are given, the remaining parameters will be determined accordingly. Therefore, in the present paper, the channel parameter d_0 and global parameter of the regenerator r_1 are chosen as independent research variables.

2.2. Gas velocity in the regenerator

In general, the gas velocity variation in the regenerator is approximately obtained by assuming a sinusoidal profile of pressure gradient [34] or velocity [56]. These methods come from the simplification of experimental results and are reasonable to some extent. However, they cannot reflect the influence of engine parameters, such as engine speed, piston phase angle, and piston stroke, on the gas velocity in the regenerator. To remedy that an approximate variation of gas average velocity in the regenerator is derived based on the piston motion and cylinder structures in this study.

The variation of expansion and compression volumes can be estimated as:

$$V_e = CVE + \frac{V_{SE}}{2}[1 + \sin(\alpha + \alpha_0 + \psi)] \tag{13}$$

$$V_c = CVC + \frac{V_{SC}}{2}[1 + \sin(\alpha + \alpha_0)] \tag{14}$$

where CVE and CVC denote the clearance volumes in the expansion chamber and the compression chamber, respectively, V_{SE} and V_{SC} represent the expansion and compression swept volumes, α and ψ are the crank angle and piston phase angle, respectively, and α_0

is the initial crank angle, which is defined as the crank angle when the engine starts.

By taking the derivative of the variation of expansion and compression volumes, the velocity variations of the two pistons are obtained as:

$$u_e = \frac{\pi B_e n}{60}\cos(\alpha + \alpha_0 + \psi) \tag{15}$$

$$u_c = \frac{\pi B_c n}{60}\cos(\alpha + \alpha_0) \tag{16}$$

where n denotes the engine speed, B_e and B_c are the piston stroke in the expansion and compression chambers, respectively.

The gas average velocity in the regenerator is approximate to the arithmetic average of the velocity of the gas flowing from the expansion chamber and the velocity of the gas flowing from the compression chamber. In actual Stirling engines, the variation of temperature and pressure for the gas in the hot part (including the expansion chamber and heater) and the cold part (including the compression chamber and cooler) is slight compared with that in the regenerator. Therefore, it can be assumed that the temperature and pressure of gas in the hot and cold parts remain unchanged with position, and then the density is kept constant in these two parts. Additionally, it is noted that the velocity of the gas flowing out of these two chambers is in the opposite direction. If the flow direction of the gas flowing from the expansion chamber is set as the positive direction, the average velocity of the gas in the regenerator can be written as:

$$u_{m,ave} = \frac{\frac{\pi B_e n}{60}\cos(\alpha + \alpha_0 + \psi)\frac{A_e \rho_e}{NA_0 \rho_{m,ave}} - \frac{\pi B_c n}{60}\cos(\alpha + \alpha_0)\frac{A_c \rho_c}{NA_0 \rho_{m,ave}}}{2} \tag{17}$$

where A_0 is the cross-section area of a single channel, A_e and A_c represent the expansion and compression swept areas, respectively, ρ_e, ρ_c, and $\rho_{m,ave}$ denote the average density of the gas in the hot part, the cold part, and the regenerator, respectively.

Assume $B_e = B_c = B$, $A_e = A_c$, then the average velocity is simplified as:

$$u_{m,ave} = \frac{\pi B n \theta d_b^2}{43200 n_r d_0^2}\left[\cos(\alpha+\alpha_0+\psi)\frac{\rho_e}{\rho_{m,ave}} - \cos(\alpha+\alpha_0)\frac{\rho_c}{\rho_{m,ave}}\right] \tag{18}$$

where d_b is the cylinder bore. In this paper, the thickness of the cylinder wall is set as 3 mm, then $d_b = 2(r_1 - 3)$ mm.

The Eq. (18) can be transformed into the following form:

$$u_{m,ave} = u_{\max}\cos(\alpha + \alpha_0 - \Lambda) \tag{19}$$

where u_{max} denotes the amplitude of the average velocity for the gas in the regenerator, Λ is the phase angle between the average velocity of the gas in the regenerator and the piston speed of the compression chamber.

$$u_{\max} = \sqrt{J_1^2 + J_2^2} \tag{20}$$

$$\Lambda = \tan^{-1}\left(\frac{J_2}{J_1}\right) \tag{21}$$

where J_1 and J_2 are calculated as:

$$J_1 = \frac{\pi B n \theta d_b^2}{43200 n_r d_0^2}\left(\frac{\rho_e}{\rho_{m,ave}}\cos\psi - \frac{\rho_c}{\rho_{m,ave}}\right) \tag{22}$$

$$J_2 = -\frac{\pi B n \theta d_b^2}{43200 n_r d_0^2}\frac{\rho_e}{\rho_{m,ave}}\sin\psi \tag{23}$$

In the above equations, the density is calculated by the ideal gas state equation. Compared with the absolute pressure, the pressure difference at various positions of the engine is little, so the following relationship is given:

$$\frac{\rho_e}{\rho_{m,ave}} = \frac{R_g T_h}{p_e} \Big/ \frac{R_g T_{m,ave}}{p_{m,ave}} \approx \frac{T_h}{T_{m,ave}} \tag{24}$$

$$\frac{\rho_c}{\rho_{m,ave}} = \frac{R_g T_c}{p_c} \Big/ \frac{R_g T_{m,ave}}{p_{m,ave}} \approx \frac{T_c}{T_{m,ave}} \tag{25}$$

where T_h and T_c denote the gas temperature in the hot part and the cold part of the engine, $T_{m,ave}$ is the gas average temperature in the regenerator, and R_g is the gas constant for helium (the working gas used in this study) and the value of it equals 2077 J/(Kg·K).

2.3. Exergy destruction analysis

In the micro-channel regenerator, the total exergy destruction rate due to the irreversibility of regenerative processes is given as:

$$\dot{E}_{xd} = \dot{E}_{xd,h} + \dot{E}_{xd,f} + \dot{E}_{xd,c} \tag{26}$$

where the three terms on the right denote the exergy destruction rate resulted from the heat transfer with a finite temperature difference, flow resistance, and axial heat conduction of solid matrix in sequence. It is worth mentioning that, under the conditions studied in this paper, the thermal conductivity of the fluid (He) is much lower than that of the solid matrix (Stainless steel, Monel 400, and Nickel-chromium), and the density of the gas and the hydraulic diameter of the regenerator channel are very small, thus the exergy destruction rate due to the axial heat conduction in the fluid can be negligible compared with the above three types of exergy destruction rates.

2.3.1. Exergy destruction rate due to heat transfer with a finite temperature difference

The regenerative process in a single micro-channel is illustrated in Fig. 3. In the discharge phase, the gas with high temperature flows from the hot part of the engines into the regenerator and releases the heat to the solid matrix. In the suction phase, the gas with low temperature flows back into the regenerator from the cold part of the engines and absorbs the heat stored in the solid matrix. As shown in Fig. 3(b), since the heat capacity of the solid matrix is much greater than that of the gas, the local temperature of the solid matrix can be considered as time-invariant and linear along the axial direction when the regenerator reaches a cyclic steady state. Consequently, the temperature profile of the solid matrix can be expressed as:

$$T_s = T_{s,c} + (T_{s,h} - T_{s,c})\frac{x}{L} \tag{27}$$

where $T_{s,h}$ and $T_{s,c}$ are the temperature of the solid matrix at the hot and cold ends, respectively, x is the axial position starting from the cold end of the regenerator. According to the assumption in Section 2.2, under the cyclic steady state, the following relationship can be given:

$$T_{s,h} = T_h \tag{28}$$

$$T_{s,c} = T_c \tag{29}$$

In Fig. 3(b), T_m is defined as the cross-sectional average temperature of the gas, which can be calculated as:

$$T_m = \frac{2}{r_0^2}\int_0^{r_0} T r dr \tag{30}$$

where r denotes the radial position, r_0 denotes the channel radius, and T denotes the local temperature of the gas in the regenerator.

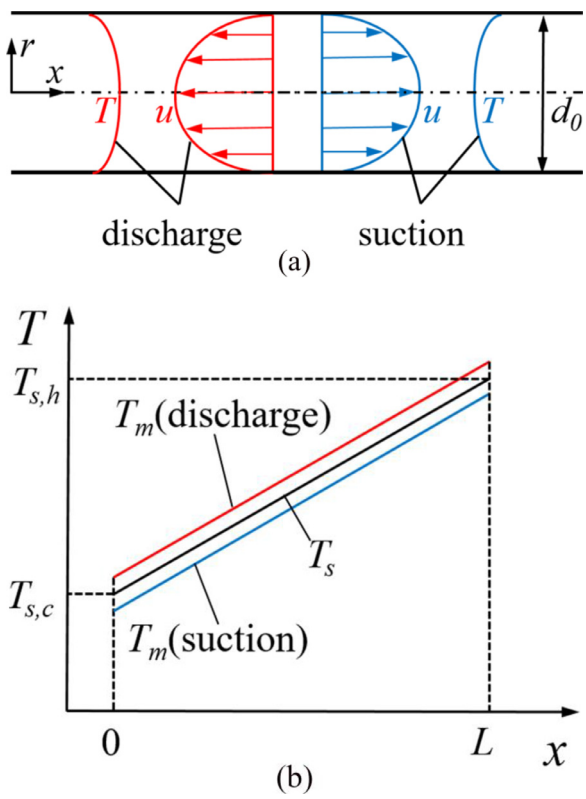

Fig. 3. Schematic of regenerative processes in a single channel for the micro-channel regenerator.

In this study, a dimensionless parameter, namely, kinetic Reynolds number Re_w, is introduced to evaluate the flow pattern in the micro-channel regenerator. The kinetic Reynolds number is calculated as $Re_\omega = \omega d_0^2 \rho_{m,ave,cyc}/\mu_{m,ave}$, where ω is the angular velocity that is defined as $\omega = \pi n/30$, $\rho_{m,ave,cyc}$ is the cyclic average density of the gas that can be calculated as $\rho_{m,ave,cyc} = p_0/R_g T_{m,ave}$ where p_0 is the charge pressure, and $\mu_{m,ave}$ is the average viscosity of the gas. It is worth noting that for most micro-channel regenerators in the actual Stirling engine, the kinetic Reynolds number is less than 1. At this point, the thermal entrance length is much smaller than the channel length and the thermal entrance effect of the gas can be ignored. Therefore, referring to the equation form of the work by Li et al. [34], the local temperature variation of the gas can be approximately determined based on the gas velocity variation given in this study.

$$T = T_c + (T_h - T_c)\left\langle \frac{d_0}{2L}\hat{x} + \frac{16F_R}{\beta \mathrm{Re}_\omega}\left\{\left[1 + \frac{7}{3}A(\hat{r}) - \frac{10}{3}X(\hat{r})\right]\cos(\alpha + \alpha_0 - \Lambda) + \left[\frac{7}{3}B(\hat{r}) - \frac{10}{3}Y(\hat{r})\right]\sin(\alpha + \alpha_0 - \Lambda)\right\}\right\rangle \tag{31}$$

where the dimensionless axial position $\hat{x}$ is defined as $\hat{x} = 2x/d_0$, the dimensionless axial position $\hat{r}$ is defined as $\hat{r} = 2r/d_0$, the relative gas displacement ratio F_R is defined as $F_R = x_{\max}/L$, and the amplitude of gas oscillation x_{max} is calculated as $x_{\max} = 2u_{\max}/\omega$. The coefficients β, $A(\hat{r})$, $B(\hat{r})$, $X(\hat{r})$, and $Y(\hat{r})$ are the non-linear combinations of zeroth-order Kelvin functions, the expressions of which are given as:

$$\beta = \frac{8}{\lambda^3}\sqrt{(\lambda - 2C_1)^2 + 4C_2^2} \tag{32}$$

$$C_1 = \frac{\mathrm{ber}\lambda\,\mathrm{bei}'\lambda - \mathrm{bei}\lambda\,\mathrm{ber}'\lambda}{\mathrm{ber}^2\lambda + \mathrm{bei}^2\lambda} \tag{33}$$

$$C_2 = \frac{\mathrm{ber}\lambda\,\mathrm{ber}'\lambda + \mathrm{bei}\lambda\,\mathrm{bei}'\lambda}{\mathrm{ber}^2\lambda + \mathrm{bei}^2\lambda} \tag{34}$$

$$A(\hat{r}) = \frac{\mathrm{ber}\lambda\,\mathrm{ber}(\lambda\hat{r}) + \mathrm{bei}\lambda\,\mathrm{bei}(\lambda\hat{r})}{\mathrm{ber}^2\lambda + \mathrm{bei}^2\lambda} \tag{35}$$

$$B(\hat{r}) = \frac{\mathrm{bei}\lambda\,\mathrm{ber}(\lambda\hat{r}) - \mathrm{ber}\lambda\,\mathrm{bei}(\lambda\hat{r})}{\mathrm{ber}^2\lambda + \mathrm{bei}^2\lambda} \tag{36}$$

$$X(\hat{r}) = \frac{\mathrm{ber}\gamma\,\mathrm{ber}(\gamma\hat{r}) + \mathrm{bei}\gamma\,\mathrm{bei}(\gamma\hat{r})}{\mathrm{ber}^2\gamma + \mathrm{bei}^2\gamma} \tag{37}$$

$$Y(\hat{r}) = \frac{\mathrm{bei}\gamma\,\mathrm{ber}(\gamma\hat{r}) - \mathrm{ber}\gamma\,\mathrm{bei}(\gamma\hat{r})}{\mathrm{ber}^2\gamma + \mathrm{bei}^2\gamma} \tag{38}$$

where ber and bei are the zeroth-order Kelvin functions, ber′ and bei′ are the first-order derivatives of ber and bei, respectively, λ denotes the Womersley number that is defined as $\lambda = \sqrt{Re_\omega}/2$, and γ denotes the modified Womersley number that is defined as $\gamma = \sqrt{Re_\omega Pr}/2$.

In addition, through the analytic study, Li et al. [34] found that when $Re_\omega \le 1$ and $Pr = 0.7$ (conformed to most of commonly used gases for actual Stirling engines), the average Nusselt number Nu between the gas and the solid matrix in the micro-channel is approximately 6, so the local heat transfer coefficient of the regenerator is:

$$h_{\alpha,x} = \frac{Nu k_m}{d_0} \approx \frac{6k_m}{d_0} \tag{39}$$

where k_m is the cross-sectional average thermal conductivity of the gas.

Therefore, the entropy generation due to the heat transfer with a finite temperature difference between the gas and the solid matrix in a single cycle for the micro-channel regenerator is given as:

$$\begin{aligned} S_{h,cyc} &= \int_0^{2\pi} Q_\alpha \left|\tfrac{1}{T_s} - \tfrac{1}{T_m}\right| \tfrac{1}{\omega} d\alpha \\ &= \int_0^{2\pi} h_\alpha |\Delta T| A \left|\tfrac{1}{T_s} - \tfrac{1}{T_m}\right| \tfrac{1}{\omega} d\alpha \\ &= \int_0^{2\pi}\int_0^{L} h_{\alpha,x} |\Delta T| \pi d_0 N \left|\tfrac{1}{T_s} - \tfrac{1}{T_m}\right| \tfrac{1}{\omega} dx d\alpha \\ &= \int_0^{2\pi}\int_0^{L} h_{\alpha,x} \tfrac{(\Delta T)^2}{T_s T_m} \pi d_0 N \tfrac{1}{\omega} dx d\alpha \\ &= \int_0^{2\pi}\int_0^{L} h_{\alpha,x} \tfrac{(\Delta T)^2}{T_s T_m} dx d\alpha \cdot \tfrac{10800 n_r d_0}{n\theta} \end{aligned} \tag{40}$$

where Q_α is the heat flux in the gas-solid interface, h_α is the average heat transfer coefficient, and ΔT is the local temperature difference between the gas and the solid matrix, which is defined as $\Delta T = T_m - T_s$.

The exergy destruction rate due to the heat transfer irreversibility of the regenerator can be determined as:

$$\dot{E}_{xd,h} = \frac{S_{h,cyc} n}{60} T_0 \tag{41}$$

where T_0 denotes the ambient temperature and is equal to 288.15 K.

2.3.2. Exergy destruction rate due to flow resistance

As the gas flows through the regenerator, a pressure drop will be generated in the gas flow. To overcome the pressure drop, a part of the available energy needs to be consumed to maintain the normal flow of the gas. The pressure drop of the gas through the circular micro-channel regenerator is given as:

$$\Delta p = \frac{1}{2} C_{f,ave} \frac{L}{d_0} \rho_{m,ave} u_{m,ave}^2 \tag{42}$$

where $C_{f,ave}$ is the average friction factor of the circular channel.

In a previous study [57], the authors found that the friction factor of the steady flow is approximate to the average of the friction

factor in the acceleration and deceleration phases of the oscillating flow. Hence, when the steady flow friction factor is used for the oscillating flow, the error of the friction factor in the acceleration and deceleration phases can offset each other. As a result, the friction factor considering the hydro-dynamical entrance effect in the steady and laminar flow [58] is introduced to calculate the pressure drop in the regenerator.

$$C_{f,ave} = \frac{64}{Re} + \frac{1.1568 d_0}{L} \tag{43}$$

where Re represents the hydraulic Reynolds number, which is defined as:

$$Re = \frac{|u_{m,ave}| d_0 \rho_{m,ave}}{\mu_{m,ave}} \tag{44}$$

Thereby, the exergy destruction resulted from the flow resistance in a single cycle of the micro-channel regenerator is given as:

$$\begin{aligned} \left(E_{xd,f}\right)_{cyc} &= \int_0^{2\pi} F|u_{m,ave}|\tfrac{1}{\omega} d\alpha \\ &= \int_0^{2\pi} \Delta p A_f |u_{m,ave}|\tfrac{1}{\omega} d\alpha \\ &= \int_0^{2\pi} \Delta p |u_{m,ave}| A_0 N \tfrac{1}{\omega} d\alpha \\ &= \int_0^{2\pi} \Delta p |u_{m,ave}| \tfrac{2700 n_r d_0^2}{n\theta} d\alpha \end{aligned} \tag{45}$$

where F denotes the total drag force of the gas, A_f is the total flow cross-section area.

The exergy destruction rate due to the flow resistance can be determined as:

$$\dot{E}_{xd,f} = \frac{\left(E_{xd,f}\right)_{cyc} n}{60} \tag{46}$$

2.3.3. Exergy destruction rate due to axial heat conduction of the solid matrix

In the regenerator, a non-negligible axial heat conduction will be caused by the large axial temperature gradient and the high effective thermal conductivity of the solid matrix. The entropy generation owing to the axial heat conduction of the solid matrix in one cycle is:

$$S_{c,cyc} = \int_0^{2\pi} \int_0^L A_s \left(\frac{\Delta T_s}{L}\right)^2 \frac{k_s^{eff}}{T_s^2} \frac{1}{\omega} dx d\alpha \tag{47}$$

where A_s denotes the cross-section area of the solid matrix, which is calculated as$A_s = \pi(1-\varphi)(r_2^2 - r_1^2)$, ΔT_s denotes the temperature difference of the solid matrix between the hot and cold ends that is defined as $\Delta T_s = T_{s,h} - T_{s,c}$, and k_s^{eff} denotes the effective thermal conductivity of the solid matrix.

For the micro-channel regenerator, when the solid matrix is a monolithic block, the effective thermal conductivity of the solid matrix k_s^{eff} is equal to the thermal conductivity of the matrix material k_s. To reduce the axial heat conduction, the regenerator is usually separated into numerous pieces along the axial direction. At this time, the effective thermal conductivity of the solid matrix will decrease due to the axial contact thermal resistance between adjacent segments. Herein, a dimensionless parameter KS is defined as the ratio of the matrix effective thermal conductivity k_s^{eff} to the material thermal conductivity k_s for evaluating the effect of solid matrix segmentation.

$$KS = \frac{k_s^{eff}}{k_s} = \frac{R_0}{R_0 + R_C} \tag{48}$$

where R_0 is the axial thermal resistance of the solid matrix without segmentation, R_C is the total axial contact thermal resistance produced by the segmentation of the solid matrix. In general, a more regenerator matrix segment means a larger total axial contact thermal resistance and thus a lower thermal conductivity ratio KS.

Table 1
Geometric dimensions of the dynamic mesh model.

Geometric parameter	Value
Piston stroke (mm)	10
Cylinder bore (mm)	3
Diameter of the flow zone (mm)	0.5
Length of the cylinder clearance (mm)	2
Length of the regenerator flow zone (mm)	10
Length of the flow straightening zone (mm)	10

The exergy destruction rate due to the axial heat conduction of the solid matrix is given as:

$$\dot{E}_{xd,c} = \frac{S_{c,cyc} n}{60} T_0 \tag{49}$$

It is worthy to mention that, for the working gas helium, the thermal conductivity and viscosity vary slightly with pressure, thus these physical properties are assumed as functions of temperature in the above analysis.

3. Comparison with CFD results

In this paper, some assumptions are made to obtain the crucial characteristics of the micro-channel regenerator such as the variations of gas velocity, friction factor, and local temperature, and Nu distribution. To ensure that the assumptions have no significant influence on the analytic results, the accuracy of these flow and thermal characteristics needs to be verified. Since the equation form of the local temperature variation and the Nu distribution used in this study have been proven in the work by Li et al. [34], only the variations of gas velocity and friction factor in the micro-channel regenerator are verified here. In this section, a numerical simulation of 3-D dynamic mesh is carried out for the circular micro-channel. The computational domain of the dynamic mesh model includes two cylinder zones, two gas flow straightening zones, and a regenerator flow zone, as illustrated in Fig. 4. The dimensions of the dynamic mesh model are listed in Table 1.

The heat transfer characteristics are not considered in the numerical simulation, so all the boundaries in the dynamic mesh model are set as the adiabatic wall. The initial temperature and pressure in the computational domain are set to be 650 K and 1 bar. A moving boundary with sinusoidal velocity variation is applied on the two piston walls using the User Defined Function (UDF). The "layering" method is selected to achieve the deformation of the dynamic mesh system. In the whole 3-D model, quadrilateral and hexahedral grids are employed. A grid independence study is performed and the results show that the friction factor in the regenerator channel of the grid system with 1.32 million grid elements varies less than 1.7% compared to that of the grid system with 0.60 million grid elements. Therefore, the grid system with 0.60 million grid elements is adopted for the calculation. The SIMPLE algorithm is employed for the pressure-velocity coupling. The standard discretization scheme is adopted for the pressure term while the second-order upwind discretization scheme is used for the other terms. The time step in the simulation is kept constant and set to 1/360 of a cycle. A residual of 1×10^{-4} for the continuity term and the momentum terms in 3 directions, and a residual of 1×10^{-7} for the energy term are set as the convergence criteria.

The variations of gas velocity and friction factor in the regenerator channel under different engine speeds and piston phase angles are obtained and compared with the approximately analytic solutions presented in this work, as plotted in Figs. 5 and 6. In Fig. 5, under different engine speeds and piston phase angles, the variation trend of gas velocity obtained by approximate analyses is similar to that obtained by the dynamic mesh simulation, especially the velocity amplitude and the corresponding crank angle

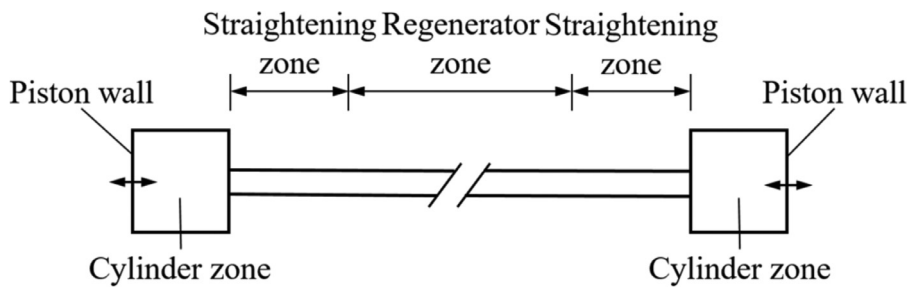

Fig. 4. Computational domain of the dynamic mesh model presented in this paper for CFD validation.

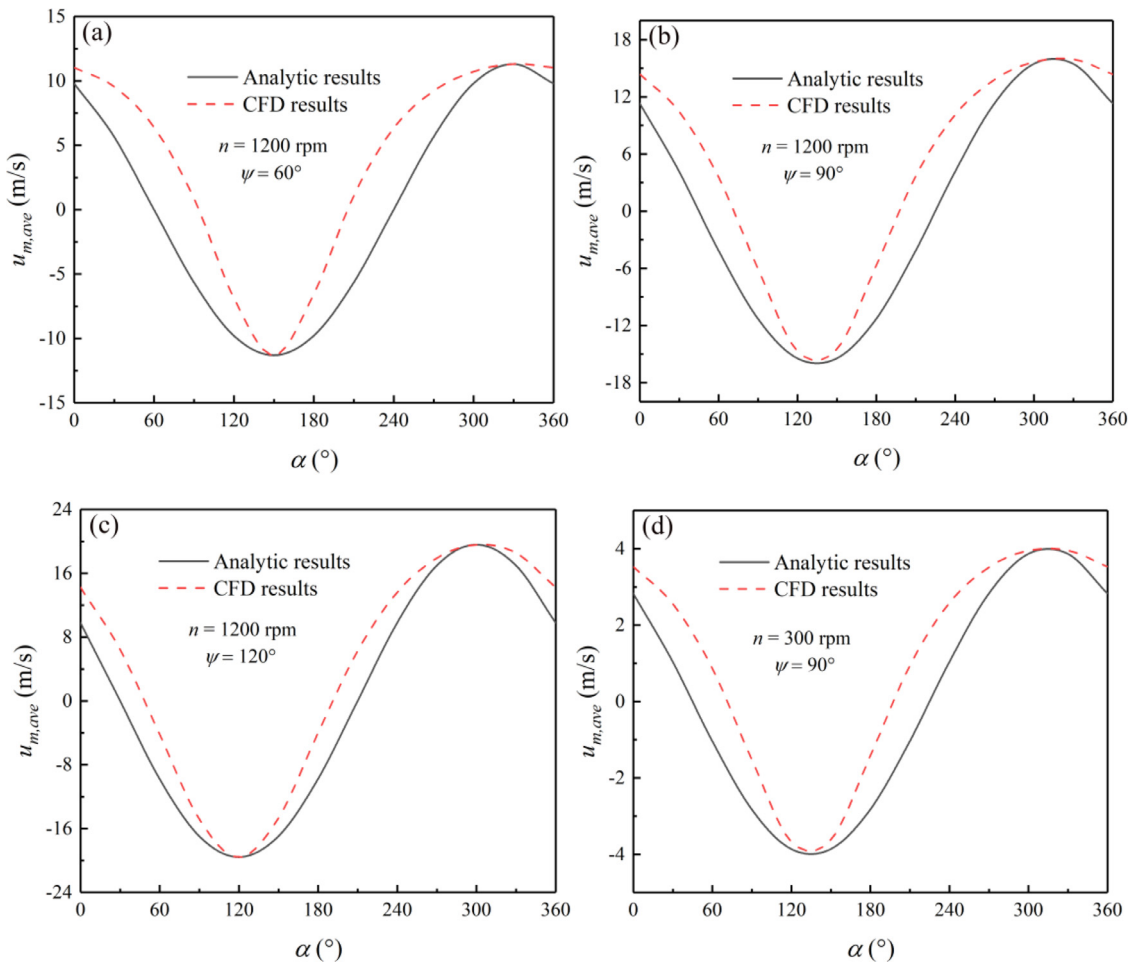

Fig. 5. Gas velocity variations in the channel under different engine speeds and piston phase angles.

of them are almost coincident. For the friction factor in Fig. 6, it can be observed that the variation trend of the analytic and CFD solutions is consistent for most parts of the cycle (R^2 = 0.9838 and 0.9442, respectively, for n = 300 rpm and 1200 rpm), except for the moments when the direction of the gas velocity in the regenerator channel changes. At the moments of changing velocity direction, the velocity profile in the channel is complex, so that a relatively large deviation will be generated if using a simple steady flow friction factor to estimate the flow resistance. However, on the whole, based on the above comparison, the variations of gas velocity and friction factor in the approximate analysis of this work are accurate and reliable.

4. Results and discussion

In the constructal design, the ranges and initial values of the main variables are summarized in Table 2. Except when being studied, the research parameters will be kept constant, with the initial values of r_1 = 50 mm, V = 6.032 × 10^5 mm^3, φ = 22.5%, n = 600 rpm, ψ = 90°, T_h = 873 K, p_0 = 4 bar, and KS = 1. Additionally, the gas temperature of the cold part T_c, initial crank angle α_0, and piston stroke B are set as the constant values of 400 K, 270°, and 75 mm. The commonly used stainless steel is selected as the material of the solid matrix, and its physical properties are set to be fixed.

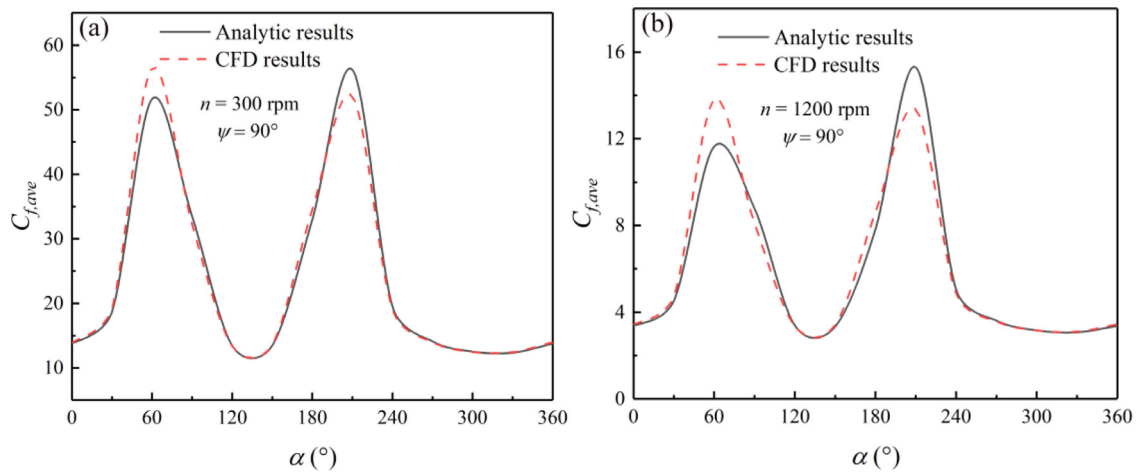

Fig. 6. Friction factor variations in the channel under different engine speeds.

Table 2
Ranges and initial values of the main variables studied in this paper.

Variable	Value range	Initial value
r_1 (mm)	30–70	50
V (mm^3)	4×10^5 – 8×10^5	6.032×10^5
φ	20–40%	22.5%
n (rpm)	300–1300	600
ψ (°)	40–140	90
T_h (K)	723–1023	873
p_0 (bar)	3–8	4
KS	0.1–1	1
d_0 (mm)	0.3–1.2	–
T_c (K)	400	–
α_0 (°)	270	–
B (mm)	75	–

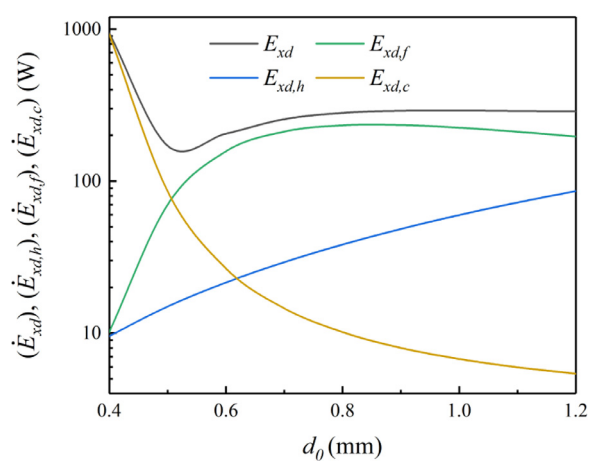

Fig. 7. Three types of exergy destruction rates and the total exergy destruction rate versus the channel diameter d_0.

Fig. 7 plots the three types of exergy destruction rates and the total exergy destruction rate versus the channel diameter d_0. It can be seen that for the regenerator with a small channel diameter, the heat transfer and flow exergy destruction rates are very low and the axial heat conduction is the main source of exergy destruction due to the large cross-section area and short length of the solid matrix. As the channel diameter increases, the total flow cross-section area decreases, due to the fixed total volume and porosity of the regenerator, the cross-section area of the solid matrix decreases and the matrix length increases, thus the axial heat conduction exergy destruction rate diminishes rapidly. However, with the increase of d_0, caused by the decrease of the total flow cross-section area, the gas velocity and pressure drop raise. Meanwhile, the total heat transfer area and coefficient will decrease, which leads to a deterioration of the heat transfer between the gas and the solid matrix. As a result, the heat transfer and flow exergy destruction rates become more significant. A maximum flow exergy destruction rate occurs at the channel diameter of around 0.85 mm. Thereafter, the pressure drop through the regenerator goes down, so the flow exergy destruction rate decreases gradually. Determined by the three types of exergy destruction rates, the total exergy destruction rate decreases firstly and then increases, and finally approaches a constant value. The total exergy destruction rate reaches its minimum under the optimal channel diameter of about 0.5 mm. At this point, the exergy destruction rate due to the axial heat conduction of the solid matrix has fallen to a very low level, while the heat transfer and flow exergy destruction rates have not increased significantly, thus leading to a minimum total exergy destruction rate.

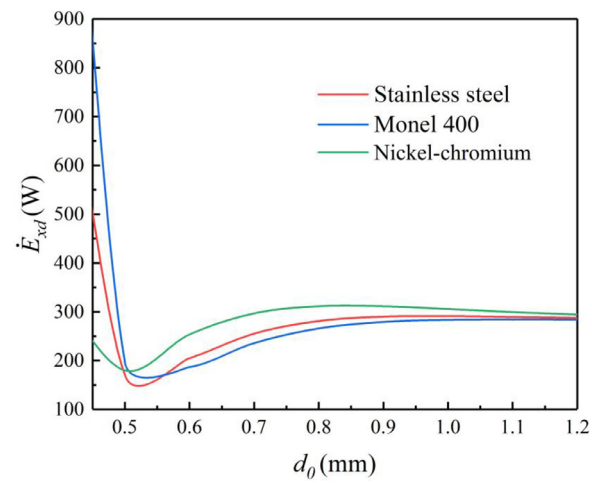

Fig. 8. Variations of the total exergy destruction rate with the channel diameter d_0 for the micro-channel regenerators with different matrix materials.

Fig. 8 shows the variation of the total exergy destruction rate with the channel diameter d_0 for the micro-channel regenerators with three different matrix materials (stainless steel, nickel-chromium, and Monel 400). It is clear that for the three different matrix materials, the total exergy destruction rate shows the

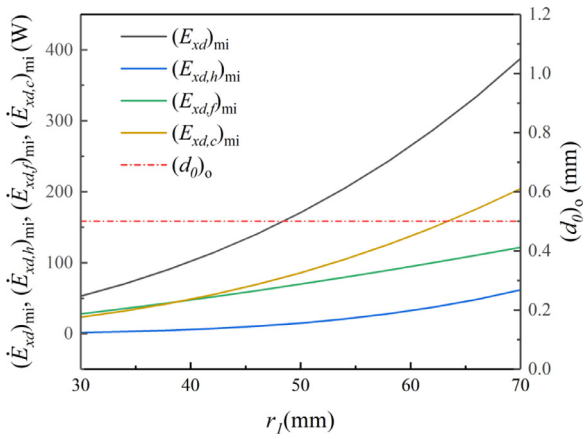

Fig. 9. Effects of the regenerator inner radius on the minimum total exergy destruction rate, its individual contributions, and the corresponding optimal channel diameter.

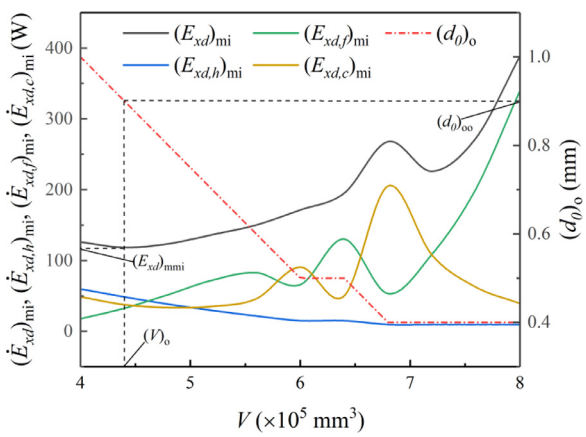

Fig. 10. Effects of the total volume of regenerators on the minimum total exergy destruction rate, its individual contributions, and the corresponding optimal channel diameter.

same variation tendency, and a similar optimal channel diameter of around 0.5 mm is obtained. Moreover, when the channel diameter $d_0 \langle$ 0.5 mm, the regenerator with the Monel 400 as matrix materials has the highest total exergy destruction rate, followed by the stainless steel and nickel-chromium. Whereas, when $d_0 \rangle$ 0.5 mm, the results are reversed. The main reasons for this phenomenon are the contrary changes of the three types of exergy destruction rates caused by the different physical properties of various matrix materials and the difference of the dominated type of exergy destruction rates under different channel diameters.

Fig. 9 depicts the effects of the regenerator inner radius r_1 on the minimum total exergy destruction rate, its individual contributions, and the corresponding optimal channel diameter $(d_0)_o$. As the regenerator inner radius increases, the contributions of all three types of exergy destruction rates increase, which leads to an increase in the minimum total exergy destruction rate. Therefore, a relatively small regenerator inner radius is recommended to be adopted to reduce the irreversible losses in the regenerator and improve the performance of Stirling engines. Nevertheless, from Fig. 9, the optimal channel diameter seems to be independent of the regenerator inner radius, with a constant value of around 0.5 mm.

Figs. 10 and 11 present the effects of the specific values of the global constraints, i.e., the total volume of regenerators V and the regenerator porosity φ, on the minimum total exergy destruction rate, its individual contributions, and the corresponding optimal channel diameter $(d_0)_o$. In Fig. 10, at a low total volume, the three irreversible losses have similar contributions to the minimum total exergy destruction rate. As the total volume increases, the heat transfer contribution decreases slowly, the axial heat conduction and flow resistance contributions fluctuate up and down and change their variation tendency frequently due to the variation of the optimal channel diameter which significantly influences the magnitude of the exergy destruction rate. However, the flow resistance contribution shows a general trend of increase. As a result, the minimum total exergy destruction rate increases with the total volume of regenerators as a whole. However, compared with the minimum total exergy destruction rate, the variation of the optimal channel diameter with the total volume of regenerators is almost reversed. Beside, a double minimum total exergy destruction rate of 118.3 W with the double optimal channel diameter $(d_0)_{oo}$ = 0.9 mm is found at the optimal total volume $(V)_o = 4.4 \times 10^5$ mm^3. From Fig. 11, it can be observed that the effect of the regenerator porosity on the constructal optimization results is nearly opposite to that of the total volume of regenerators. As well, the total exergy destruction rate has its double minimum of 97.4 W with an optimal regenerator porosity $(\varphi)_o$ = 36% and a double optimal channel diameter $(d_0)_{oo}$ = 1.1 mm. The results in Figs. 10 and 11 indicate that the global structure constraints of the regenerator have a significant influence on the regenerator performance, and they should be taken into account in the engine design.

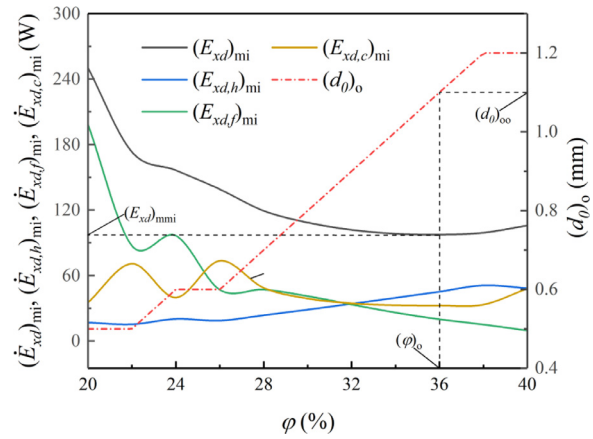

Fig. 11. Effects of the regenerator porosity on the minimum total exergy destruction rate, its individual contributions, and the corresponding optimal channel diameter.

The relationships between the main operating parameters of Stirling engines, i.e., engine speed n, piston phase angles ψ, hot part temperature T_h and charge pressure p_0, and the optimization results are illustrated in Figs. 12–15. As can be seen in Fig. 12, the minimum total exergy destruction rate increases first and then decreases with the rise of the engine speed, exhibiting a peak value at the engine speed n of around 1100 rpm. The alternative changes of the flow resistance and the axial heat conduction contributions with opposite trends jointly determine the variation of the minimum total exergy destruction rate. According to Figs. 13–15, the minimum total exergy destruction rate increases with the piston phase angle, hot part temperature, and charge pressure in the whole research range. When the piston phase angle $\psi \langle 60^\circ$ or $\psi \rangle 70^\circ$, the change in the flow resistance contribution is the main cause for the increase in the minimum total exergy destruction rate, while at $60^\circ < \psi < 70^\circ$, the increase in the minimum total exergy destruction rate mostly comes from the augment in the axial heat conduction contribution. As the hot part temperature increases, three types of contributions of irreversible losses raise at different rates, leading to the increase of the minimum total ex-

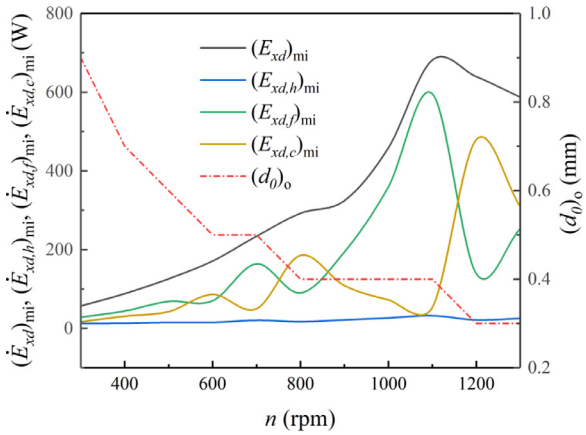

Fig. 12. Effects of the engine speed on the minimum total exergy destruction rate, its individual contributions, and the corresponding optimal channel diameter.

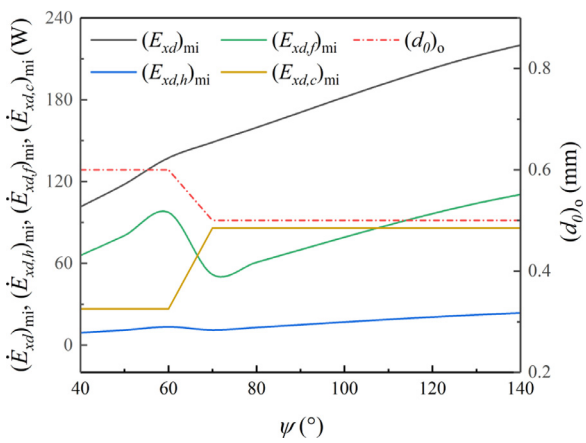

Fig. 13. Effects of the piston phase angle on the minimum total exergy destruction rate, its individual contributions, and the corresponding optimal channel diameter.

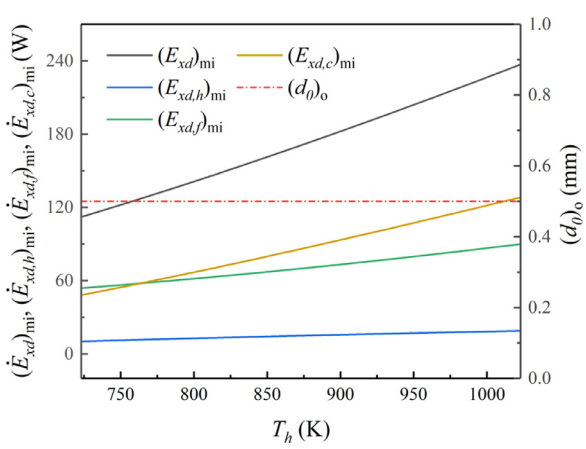

Fig. 14. Effects of the hot part temperature on the minimum total exergy destruction rate, its individual contributions, and the corresponding optimal channel diameter.

ergy destruction rate. However, interestingly, with the increase of the charge pressure, only the heat transfer contribution raises correspondingly, while the other two types of contributions are kept constant. This is because when the charge pressure increases, the gas density will increase, but the average velocity and pressure drop of the gas through the regenerator and the axial heat conduction of the solid matrix are independent of the gas density, thus the exergy destruction rates resulted from the flow resistance and

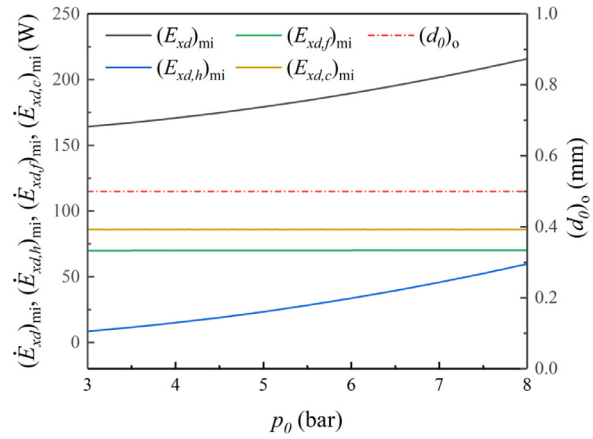

Fig. 15. Effects of the charge pressure on the minimum total exergy destruction rate, its individual contributions, and the corresponding optimal channel diameter.

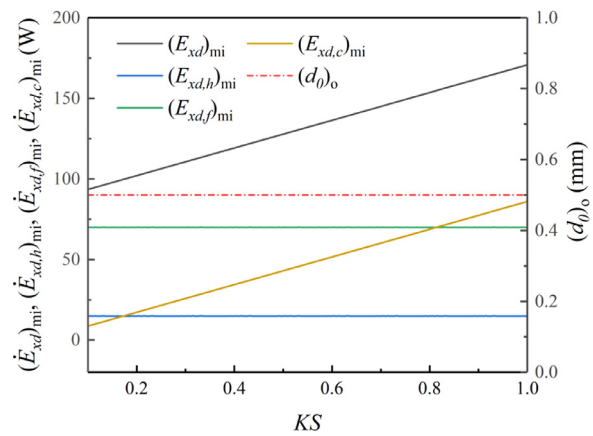

Fig. 16. Effects of the thermal conductivity ratio on the minimum total exergy destruction rate, its individual contributions, and the corresponding optimal channel diameter.

the axial heat conduction are fixed. In addition, from Figs. 12–15, it is clear that the engine speed has an evident effect on the optimal channel diameter $(d_0)_o$, but the influence of the piston phase angle, hot part temperature, and charge pressure on the optimal channel diameter is not obvious.

To observe the effects of the thermal conductivity ratio *KS* on the irreversibility of the micro-channel regenerator, Fig. 16 presents the characteristics of the minimum total exergy destruction rate, its individual contributions, and the corresponding optimal channel diameter $(d_0)_o$ versus the thermal conductivity ratio. It is clear that, as the segments of the regenerator increase, the thermal conductivity ratio decreases, which leads to the decrease of the axial heat conduction contribution, thus the minimum total exergy destruction rate will be reduced. It illustrates that the performance of the micro-channel regenerator can be further improved by the segmentation of the regenerator and more segments mean higher regenerator performance. Furthermore, the optimal channel diameter is shown to be invariable as the thermal conductivity ratio changes.

5. Conclusion

With the fixed total volume and porosity, the structures of the circular micro-channel regenerator were optimized based on constructal theory in this paper. The minimum total exergy destruction rate and the corresponding optimal channel diameter were obtained, and the effects of some important geometric and struc-

tural parameters on the optimization results were analyzed. The major conclusions can be drawn as follows:

1 As the channel diameter d_0 increases, the exergy destruction rate due to the axial heat conduction of the solid matrix decreases at a speed significantly larger than the increases of the exergy destruction rates due to the heat transfer with a finite temperature difference and the flow resistance, which leads to a minimum total exergy destruction rate at a relatively low channel diameter $d_0 = 0.5$ mm for the regenerators with different matrix materials.
2 With the decreases of the regenerator inner radius r_1, total volume V and thermal conductivity ratio KS, and the increase of the regenerator porosity φ, the minimum total exergy destruction rate decreases as a whole. A double minimum total exergy destruction rate of 118.3 W with the double optimal channel diameter $(d_0)_{oo} = 0.9$ mm and a double minimum total exergy destruction rate of 97.4 W with the double optimal channel diameter $(d_0)_{oo} = 1.1$ mm are achieved under the optimal total volume $(V)_o = 4.4 \times 10^5$ mm^3 and the optimal regenerator porosity $(\varphi)_o = 36\%$, respectively.
3 The minimum total exergy destruction rate decreases with the decreases in the engine speed n, piston phase angle ψ, hot part temperature T_h, and charge pressure p_0, which means that the regenerator performance can be further improved by selecting appropriate operating parameters of engines. In this study, a maximum of 97% reduction in the total exergy destruction rate is obtained after constructal optimization. However, since these operating parameters will directly influence the ideal performance of the engines, the specific parameter selection needs to be considered in combination with the evaluation under the engine level.
4 According to the effects of the parameters on the optimal channel diameter, it can be concluded that the engine speed n and the important geometric parameters such as the regenerator inner radius r_1, total volume V and regenerator porosity φ have a significant influence on the optimal structure of the microchannel regenerator, while when the piston phase angle ψ, hot part temperature T_h, charge pressure p_0, and thermal conductivity ratio KS changes, the optimal structure of the regenerator will be almost unaffected by them.

Declaration of Competing Interest

None.

CRediT authorship contribution statement

Minjie Yu: Conceptualization, Methodology, Software, Validation, Formal analysis, Investigation, Data curation, Writing – original draft, Writing – review & editing, Visualization. **Chunyu Shi:** Methodology, Software, Writing – review & editing. **Junhao Xie:** Methodology, Software, Formal analysis. **Peng Liu:** Methodology, Software, Formal analysis, Resources, Funding acquisition. **Zhichun Liu:** Conceptualization, Writing – review & editing, Resources, Supervision, Project administration, Funding acquisition. **Wei Liu:** Conceptualization, Writing – review & editing, Resources, Supervision, Project administration, Funding acquisition.

Acknowledgements

This work was supported by the National Natural Science Foundation of China (Grant No. 51736004) and the China Postdoctoral Science Foundation (Grant No. 2020M672344).

References

[1] S. Alfarawi, R. Al-Dadah, S. Mahmoud, Influence of phase angle and dead volume on gamma-type Stirling engine power using CFD simulation, Energy Convers. Manag. 124 (2016) 130–140.
[2] A. Abuelyamen, R. Ben-Mansour, H. Abualhamayel, E.M.A. Mokheimer, Parametric study on beta-type Stirling engine, Energy Convers. Manag. 145 (2017) 53–63.
[3] R. Li, L. Grosu, D. Queiros-Condé, Losses effect on the performance of a Gamma type Stirling engine, Energy Convers. Manag. 114 (2016) 28–37.
[4] W.L. Chen, K.L. Wong, Y.F. Chang, A numerical study on the effects of moving regenerator to the performance of a β -type Stirling engine, Int. J. Heat Mass Transf. 83 (2015) 499–508.
[5] A.R. Tavakolpour, A. Zomorodian, A. Akbar Golneshan, Simulation, construction and testing of a two-cylinder solar Stirling engine powered by a flat-plate solar collector without regenerator, Renew. Energy 33 (1) (2008) 77–87.
[6] S.C. Costa, H. Barrutia, J.A. Esnaola, M. Tutar, Numerical study of the pressure drop phenomena in wound woven wire matrix of a Stirling regenerator, Energy Convers. Manag. 67 (2013) 57–65.
[7] M. Ni, H. Peng, U. Sultan, K. Luo, G. Xiao, A quantitative method to describe the flow characteristics of an oscillating flow including porous media, Int. J. Heat Mass Transf. 119 (2018) 860–866.
[8] G. Xiao, H. Peng, H. Fan, U. Sultan, M. Ni, Characteristics of steady and oscillating flows through regenerator, Int. J. Heat Mass Transf. 108 (2017) 309–321.
[9] M. Tanaka, I. Yamashita, F. Chisaka, Flow and heat transfer characteristics of the Stirling engine regenerator in an oscillating flow, JSME Int. J. 33 (2) (1990) 283–289.
[10] S.C. Costa, M. Tutar, I. Barreno, J.A. Esnaola, H. Barrutia, D. García, M.A. González, J.I. Prieto, Experimental and numerical flow investigation of Stirling engine regenerator, Energy 72 (2014) 800–812.
[11] S. Isshiki, Y. Takasaki, I. Ushiyama, An experimental study on flow resistance of regenerator wire meshes in oscillatory flow, in: Proceedings of the 32nd Intersociety Conference of Energy Conversion Engineering, 1997, pp. 1027–1032.
[12] S.C. Costa, H. Barrutia, J.A. Esnaola, M. Tutar, Numerical study of the heat transfer in wound woven wire matrix of a Stirling regenerator, Energy Convers. Manag. 79 (2014) 255–264.
[13] S.K. Andersen, H. Carlsen, P.G. Thomsen, Preliminary results from simulations of temperature oscillations in Stirling engine regenerator matrices, Energy 31 (10–11) (2006) 1371–1383.
[14] S.K. Andersen, H. Carlsen, P.G. Thomsen, Numerical study on optimal Stirling engine regenerator matrix designs taking into account the effects of matrix temperature oscillations, Energy Convers. Manag. 47 (7–8) (2006) 894–908.
[15] R. Gheith, F. Aloui, S.Ben Nasrallah, Study of temperature distribution in a Stirling engine regenerator, Energy Convers. Manag. 88 (2014) 962–972.
[16] B. Rutczyk, I. Szczygieł, A. Kabaj, Evaluation of an α type stirling engine regenerator using a new differential model, Energy 209 (2020) 118369.
[17] D. Gedeon, J.G. Wood, Oscillating-flow Regenerator Test Rig: Hardware and Theory with Derived Correlations for Screens and Felts, NASA, 1996 CR-198442.
[18] P. Bitsikas, E. Rogdakis, G. Dogkas, CFD study of heat transfer in Stirling engine regenerator, Therm. Sci. Eng. Prog. 17 (2020) 100492.
[19] Z. Buliński, A. Kabaj, T. Krysiński, I. Szczygieł, W. Stanek, B. Rutczyk, L. Czarnowska, P. Gładysz, A computational fluid dynamics analysis of the influence of the regenerator on the performance of the cold Stirling engine at different working conditions, Energy Convers. Manag. 195 (2019) 125–138.
[20] W.L. Chen, K.L. Wong, H.E. Chen, An experimental study on the performance of the moving regenerator for a γ-type twin power piston Stirling engine, Energy Convers. Manag. 77 (2014) 118–128.
[21] D.D. Dai, F. Yuan, R. Long, Z.C. Liu, W. Liu, Imperfect regeneration analysis of Stirling engine caused by temperature differences in regenerator, Energy Convers. Manag. 158 (2018) 60–69.
[22] R. Gheith, F. Aloui, S.Ben Nasrallah, Determination of adequate regenerator for a Gamma-type Stirling engine, Appl. Energy 139 (2015) 272–280.
[23] Y. Kato, Indicated diagrams of low temperature differential Stirling engines with channel-shaped heat exchangers, Renew. Energy 103 (2017) 30–37.
[24] A.S. Nielsen, B.T. York, B.D. MacDonald, Stirling engine regenerators: how to attain over 95% regenerator effectiveness with sub-regenerators and thermal mass ratios, Appl. Energy 253 (2019) 113557.
[25] Z. Li, Y. Haramura, Y. Kato, D. Tang, Analysis of a high performance model Stirling engine with compact porous-sheets heat exchangers, Energy 64 (2014) 31–43.
[26] M.B. Ibrahim, D. Danila, T. Simon, S. Mantell, L.Y. Sun, A Microfabricated Segmented-involute-foil Regenerator for Enhancing Reliability and Performance of Stirling Engines: Phase II Final Report for the Radioisotope Power Conversion Technology NRA Contract NAS3-03124, Mechanical Engineering Faculty Publications, 2007 December.
[27] R. Tew, M. Ibrahim, D. Danila, T. Simon, S. Mantell, L. Sun, D. Gedeon, K. Kelly, J. McLean, J. Wood, S. Qiu, A microfabricated involute-foil regenerator for Stirling engines, in: Proceedings of the International Energy Conversion Engineering Conference and Exhibit, St. Louis, Missouri, 2007, pp. 1–25.
[28] K. Nam, S. Jeong, Development of parallel wire regenerator for cryocoolers, Cryogenics 46 (4) (2006) 278–287 (Guildf).
[29] S. Isshiki, H. Sato, S. Konno, H. Shiraishi, N. Isshiki, L. Fujii, H. Mizui, The experimental study of atmospheric Stirling engines using pin-fin arrays' heat exchangers, J. Power Energy Syst. 2 (2008) 1198–1208.
[30] H. Wang, B. Zhang, M. Liu, Z. Rao, Analytical solution of heat transfer perfor-

mance of pin-array stack regenerator in Stirling cycle, Int. J. Therm. Sci. 167 (2021) 107015.
[31] K. Yanaga, R. Li, S. Qiu, Robust foil regenerator flow loss and heat transfer tests under oscillating flow condition, Appl. Therm. Eng. 178 (2020) 115525.
[32] S. Alfarawi, R. Al-Dadah, S. Mahmoud, Transient investigation of mini-channel regenerative heat exchangers: combined experimental and CFD approach, Appl. Therm. Eng. 125 (2017) 346–358.
[33] S. Alfarawi, R. Al-Dadah, S. Mahmoud, Potentiality of new miniature-channels Stirling regenerator, Energy Convers. Manag. 133 (2017) 264–274.
[34] Z. Li, Y. Haramura, D. Tang, C. Guo, Analysis on the heat transfer characteristics of a micro-channel type porous-sheets Stirling regenerator, Int. J. Therm. Sci. 94 (2015) 37–49.
[35] S.K. Garg, B. Premachandran, M. Singh, S. Sachdev, M. Sadana, Effect of Porosity of the regenerator on the performance of a miniature Stirling cryocooler, Therm. Sci. Eng. Prog. 15 (2020) 100442.
[36] A. Bejan, Constructal-theory network of conducting paths for cooling a heat generating volume, Int. J. Heat Mass Transf. 40 (4) (1997) 799–816.
[37] A. Bejan, S. Lorente, Constructal theory of generation of configuration in nature and engineering, J. Appl. Phys. 100 (4) (2006) 041301.
[38] L. Chen, Q. Xiao, Z. Xie, F. Sun, Constructal entransy dissipation rate minimization for tree-shaped assembly of fins, Int. J. Heat Mass Transf. 67 (2013) 506–513.
[39] H. Feng, L. Chen, Z. Xie, F. Sun, Constructal design for helm-shaped fin with internal heat sources, Int. J. Heat Mass Transf. 110 (2017) 1–6.
[40] G. Lorenzini, E. da Silva Diaz Estrada, E.D. dos Santos, L.A. Isoldi, L.A.O. Rocha, Constructal design of convective cavities inserted into a cylindrical solid body for cooling, Int. J. Heat Mass Transf. 83 (2015) 75–83.
[41] J. Lee, Y. Kim, S. Lorente, A. Bejan, Constructal design of a comb-like channel network for self-healing and self-cooling, Int. J. Heat Mass Transf. 66 (2013) 898–905.
[42] H. Feng, L. Chen, Z. Xie, F. Sun, Constructal entropy generation rate minimization for X-shaped vascular networks, Int. J. Therm. Sci. 92 (2015) 129–137.
[43] B.C. Feijó, G. Lorenzini, L.A. Isoldi, L.A.O. Rocha, J.N.V. Goulart, E.D. dos Santos, Constructal design of forced convective flows in channels with two alternated rectangular heated bodies, Int. J. Heat Mass Transf. 125 (2018) 710–721.
[44] H. Feng, Z. Xie, L. Chen, Z. Wu, S. Xia, Constructal design for supercharged boiler superheater, Energy 191 (2020) 116484.
[45] H. Feng, L. Chen, S. Xia, Constructal design for disc-shaped heat exchanger with maximum thermal efficiency, Int. J. Heat Mass Transf. 130 (2019) 740–746.
[46] A. Bejan, S. Lorente, J. Lee, Y. Kim, Constructal design of gas-cooled electric power generators, self-pumping and atmospheric circulation, Int. J. Heat Mass Transf. 91 (2015) 647–655.
[47] E. Norouzi, M. Amidpour, M. Rezakazemi, Heat recovery steam generator: constructal thermoeconomic optimization, Appl. Therm. Eng. 148 (2019) 747–753.
[48] Z. Wu, H. Feng, L. Chen, Z. Xie, C. Cai, S. Xia, Optimal design of dual-pressure turbine in OTEC system based on constructal theory, Energy Convers. Manag. 201 (2019) 112179.
[49] P.V. Trevizoli, J.R. Barbosa, Entropy generation minimization analysis of oscillating-flow regenerators, Int. J. Heat Mass Transf. 87 (2015) 347–358.
[50] V.A.F. Costa, On the exergy balance equation and the exergy destruction, Energy 116 (2016) 824–835.
[51] A. Bejan, Advanced Engineering Thermodynamics, John Wiley & Sons, 2016.
[52] W. Liu, P. Liu, J.B. Wang, N.B. Zheng, Z.C. Liu, Exergy destruction minimization: a principle to convective heat transfer enhancement, Int. J. Heat Mass Transf. 122 (2018) 11–21.
[53] L. Silva-Llanca, S. Inostroza-Lagos, Optimum power generation assessment in an H-Darrieus vertical axis wind turbine via exergy destruction minimization, Energy Convers. Manag. 243 (2021) 114312.
[54] J.Y. Lv, Z.C. Liu, W. Liu, Active design for the tube insert of center-connected deflectors based on the principle of exergy destruction minimization, Int. J. Heat Mass Transf. 150 (2020) 119260.
[55] R. Gupta, S. Asgari, H. Moazamigoodarzi, S. Pal, I.K. Puri, Cooling architecture selection for air-cooled data centers by minimizing exergy destruction, Energy 201 (2020) 117625.
[56] I. Barreno, S.C. Costa, M. Cordon, M. Tutar, I. Urrutibeascoa, X. Gomez, G. Castillo, Numerical correlation for the pressure drop in Stirling engine heat exchangers, Int. J. Therm. Sci. 97 (2015) 68–81.
[57] M. Yu, F. Xin, X. Lai, H. Xiao, Z. Liu, W. Liu, Study of oscillating flows through a novel constructal bifurcation Stirling regenerator, Appl. Therm. Eng. 184 (2021) 116413.
[58] Z.Q. Wang, Study on correction coefficients of laminar and turbulent entrance region effect in round pipe, Appl. Math. Mech. 3 (1982) 434–446.